

Gated Graph Recurrent Neural Networks

Luana Ruiz, Fernando Gama and Alejandro Ribeiro

Abstract—Graph processes exhibit a temporal structure determined by the sequence index and a spatial structure determined by the graph support. To learn from graph processes, an information processing architecture must then be able to exploit both underlying structures. We introduce Graph Recurrent Neural Networks (GRNNs), which achieve this goal by leveraging the hidden Markov model (HMM) together with graph signal processing (GSP). In the GRNN, the number of learnable parameters is independent of the length of the sequence and of the size of the graph, guaranteeing scalability. We also prove that GRNNs are permutation equivariant and that they are stable to perturbations of the underlying graph support. Following the observation that stability decreases with longer sequences, we propose a time-gated extension of GRNNs. We also put forward node- and edge-gated variants of the GRNN to address the problem of vanishing gradients arising from long range graph dependencies. The advantages of GRNNs over GNNs and RNNs are demonstrated in a synthetic regression experiment and in a classification problem where seismic wave readings from a network of seismographs are used to predict the region of an earthquake. Finally, the benefits of time, node and edge gating are experimentally validated in multiple time and spatial correlation scenarios.

Index Terms—graph recurrent neural networks, graph convolutions, gating, stability, graph signal processing

I. INTRODUCTION

Neural networks are powerful nonlinear parametrizations whose success has been demonstrated in an array of applications, from speech recognition [2], [3] and image classification [4] to weather forecasting [5] and ECG analysis [6]. Their popularity can be explained by many different reasons, but it is mainly related to the remarkable performance that *structured* neural networks such as convolutional neural networks (CNNs) [7]–[9], graph neural networks (GNNs) [10]–[12] and recurrent neural networks (RNNs) [13]–[15] have achieved in recent years [16]. What these three architectures have in common is that they are *adapted* to the data structures that they process. *CNNs* extract shared features across different regions of an image by replacing arbitrary linear transforms with compositions of convolution and pooling operations; *convolutional GNNs* take local graph structures into account by extending these CNN operations to their graph counterparts; and *RNNs* learn causal dependencies in sequential data by leveraging the recurrence relationship of a hidden Markov model (HMM).

As powerful as they are, all of these architectures handle data that exhibits only one type of structure, either temporal

or spatial. *Graph processes*, however, are temporal sequences of graph signals, and as such contain both a time dimension, reflected by the indices of the sequence, and a graph structure inherent to the graph signals. In the context of learning, graph processes have been used to model data such as weather variables on weather station networks [17] and seismic wave readings on a network of seismographs [18]. While a GNN is fit to operate on such data, it either requires processing one instant at a time or considering multiple time instants as features of the signal, in both cases effacing the temporal relationship between samples. Likewise, a RNN must either consider all nodes as features of the process –thus ignoring the graph structure altogether– or pre-process the data using graph embeddings, which are costly and entail loss of structural information.

In this paper, we introduce a Graph Recurrent Neural Network (GRNN) architecture that takes both the graph and temporal dimensions of a graph process into account. Retaining the same recurrence relation implemented by RNNs, in Section III we propose replacing the input-to-state and state-to-state linear transformation of the HMM by graph convolutions [19], which not only take the graph structure into account but also guarantee equivariance to node relabelings and make the number of parameters independent of the size of the graph [20]. In Section IV, we prove that GRNNs also exhibit stability to relative perturbations of the underlying graph, meaning that changes in the output caused by changes in the graph are bounded by the size of the perturbation [21]. We observe that the stability of GRNNs deteriorates with increased sequence length. To address this, in Section V we propose gating mechanisms that allow the GRNN architecture to successfully encode long term temporal dependencies and long range spatial dependencies.

GRNNs process input sequences of arbitrary length, taking in long processes as a whole, or split in a series of shorter sequences to increase the number of gradient updates within the process. They are also flexible in terms of the shape of the output signal, which can be anything from a class label to a series of labels, a signal to a series of signals, supported on a graph or not. Related work on GRNNs [22]–[25] considers only regression problems and is thus limited to outputting sequences of graph signals, with [22]–[24] targeting traffic forecasting specifically. Other somewhat related works include the gated graph sequence neural networks [26] and the recurrent formulation in [27]. The architecture in [26] learns sequential representations from graphs, and not from graph signals or processes; this is a fundamental difference, since in learning from graphs the graph is seen as data, while in learning from graph signals the graph is given (i.e. a hyperparameter of the learning architecture). The work in [27] uses recurrence as a means of re-introducing the input at

The work in this paper was supported by NSF CCF 1717120, ARO W911NF1710438, ARL DCIST CRA W911NF-17-2-0181, ISTC-WAS and Intel DevCloud. Preliminary results appear at the EUSIPCO19 conference [1]. L. Ruiz, F. Gama and A. Ribeiro are with the Dept. of Electrical and Systems Eng., Univ. of Pennsylvania. Email: {rubruiz,fgama,aribeiro}@seas.upenn.edu.

every layer to capture multiple types of diffusion, but does not consider data consisting of temporal sequences. While *time gating* has been discussed in [22]–[26], the novel *spatial gating strategies* that we put forward leverage the graph's *node* and *edge structures* to control how long range spatial dependencies on the graph are encoded. Finally, we note that our manuscript presents a novel stability analysis of GRNNs, which both elucidates the effect of the sequence length on stability and motivates the need for gating.

The remaining sections of this paper are organized as follows. Section II goes over RNNs and graph signal processing. Following the introduction of GRNNs in Section III, in Section IV we analyze their stability and in Section V introduce Gated GRNNs. In Section VI, we evaluate the performance of all proposed architectures on a synthetic k -step prediction experiment and on a real-world experiment involving seismic data, where the GRNN architectures are also compared with GNNs and RNNs. Concluding remarks are presented in Section VII.

II. RECURRENT NEURAL NETWORKS AND GRAPH DATA

Instrumental to the design of GRNNs are the concepts of traditional RNNs as models of sequential data as well as the framework of graph signal processing. Thus, we introduce the HMM model approximation for sequential data and discuss how RNNs can be used to process them (Section II-A), and we follow with an overview of graph signals, graph convolutions and graph processes (Section II-B).

A. Recurrent Neural Networks (RNNs)

Let $\{\mathbf{x}_t\}_{t \in \mathbb{N}_0}$ be a sequence of N -dimensional data points $\mathbf{x}_t \in \mathbb{R}^N$. The elements of this sequence are related to one another through a *causal relationship* $\mathbf{x}_t = \phi(\mathbf{x}_{t-1}, \mathbf{x}_{t-2}, \dots)$, where the map ϕ is unknown. To process the information carried by this sequence, we need to *learn* the causal relationship ϕ . In recurrent neural networks (RNNs), this is done by approximately modeling ϕ as a HMM. In the HMM, $\mathbf{x}_{t+1} \approx \varphi(\mathbf{x}_t, \mathbf{z}_t)$, where $\{\mathbf{z}_t\}_{t \in \mathbb{N}_0}$ is a sequence of hidden states $\mathbf{z}_t \in \mathbb{R}^N$. We point out that, while it is not necessary for \mathbf{z}_t and \mathbf{x}_t to share the same dimensions (in most realizations of RNNs, they often do not), we assume so here for the sake of argument and ease of exposition.

The hidden states \mathbf{z}_t are learned from the sequence $\{\mathbf{x}_t\}_{t \in \mathbb{N}_0}$ using a nonlinear map that takes the current datapoint \mathbf{x}_t and the previous hidden state \mathbf{z}_{t-1} as inputs, and outputs the updated hidden state \mathbf{z}_t . This map is parametrized as

$$\mathbf{z}_t = \sigma(\mathbf{A}\mathbf{x}_t + \mathbf{B}\mathbf{z}_{t-1}) \quad (1)$$

where $\mathbf{A} \in \mathbb{R}^{N \times N}$ and $\mathbf{B} \in \mathbb{R}^{N \times N}$ are linear operators and $\sigma : \mathbb{R} \rightarrow \mathbb{R}$ is a pointwise nonlinearity, i.e. $[\sigma(\mathbf{x})]_i = \sigma([\mathbf{x}]_i)$.

The sequence $\{\mathbf{x}_t\}$ is typically accompanied by a target representation \mathcal{Y} , which can be seen as a more appropriate representation of $\{\mathbf{x}_t\}$ for the task at hand. The elements of \mathcal{Y} could be, for instance, a single value $y \in \mathcal{Y}$ to summarize information from the entire sequence, like a sentiment describing a tweet [28]; or, they could be another sequence $\{\mathbf{y}_t\}_{t \in \mathbb{N}_0}$, $\mathbf{y}_t \in \mathbb{R}^M$, which is the case in automatic speech recognition

[2]. RNNs estimate \mathcal{Y} by applying a second nonlinear map, $\Phi : \mathbb{R}^N \rightarrow \mathbb{R}^M$, to the hidden state. In the case where the target representation is a sequence, this map is parametrized as

$$\Phi(\mathbf{z}_t) = \rho(\mathbf{C}\mathbf{z}_t) \quad (2)$$

where $\mathbf{C} \in \mathbb{R}^{M \times N}$ is the linear *output* map and $\rho : \mathbb{R} \rightarrow \mathbb{R}$ is the pointwise nonlinearity used to compute the output, $[\rho(\mathbf{x})]_i = \rho([\mathbf{x}]_i)$. In cases where a single output value y is associated with the sequence $\{\mathbf{x}_t\}$, we can estimate y from the state at the end T of the sequence, $\Phi(\mathbf{z}_T) = \rho(\mathbf{C}\mathbf{z}_T)$.

Given a training set $\{(\{\mathbf{x}_t\}, \mathcal{Y})\}$ comprised of several sequences $\{\mathbf{x}_t\}$ and their associated representations \mathcal{Y} , the optimal linear maps \mathbf{A} , \mathbf{B} and \mathbf{C} are obtained by minimizing some loss function $\mathcal{L}(\Phi(\mathbf{z}_t), \mathcal{Y})$ (or $\mathcal{L}(\Phi(\mathbf{z}_T), \mathcal{Y})$) over the training set. This joint learning framework makes the hidden state adaptable to the task at hand, exploiting the available training examples to determine which pieces of sequential information are relevant to store in the hidden state \mathbf{z}_t .

Key to the success of RNNs is the fact that the number of parameters (entries) in the linear operators \mathbf{A} , \mathbf{B} and \mathbf{C} *do not* depend on the time index t . In other words, the same linear operators are applied throughout the entire sequence. This parameter-sharing scheme across the time-dimension has two main advantages: it keeps the number of parameters under control and, simultaneously, allows learning from sequences of variable length. This is consistent with the HMM approximation model, where each *learned* state only depends on the current input and on the previous state. Regardless of the start time t_0 , as long as the current value of the input and of the previous state are the same, the updated state will always be the same. The parameter-sharing scheme is thus an effective way by which RNNs are able to exploit the structure imposed by the HMM.

B. Graph data

In upcoming sections, our focus will be on adapting RNNs to process *graph data*. Let $\mathcal{G} = (\mathcal{V}, \mathcal{E}, \mathcal{W})$ be a graph, where $\mathcal{V} = \{1, \dots, N\}$ is the set of nodes, $\mathcal{E} \subseteq \mathcal{N} \times \mathcal{N}$ is the set of edges and $\mathcal{W} : \mathcal{E} \rightarrow \mathbb{R}$ is a weight function assigning proximity weights to the edges in \mathcal{E} . We say that a data sample \mathbf{x} is a *graph signal* [29], [30] if its entries are related through the graph \mathcal{G} . To be more precise, each node $n \in \mathcal{V}$ is assigned an entry $[\mathbf{x}]_n = x_n$, and any two entries x_i and x_j are presumed related if there is an edge between them. The *strength* of this relationship is usually measured by the edge weight.

To provide a better interpretation of the relationship between the signal \mathbf{x} and the graph \mathcal{G} , we define the graph shift operator (GSO) $\mathbf{S} \in \mathbb{R}^{N \times N}$ as a matrix that encodes the sparsity pattern of \mathcal{G} by requiring that entries $[\mathbf{S}]_{ij} = s_{ij}$ be nonzero only if $i = j$ or $(j, i) \in \mathcal{E}$. The value s_{ij} reflects the influence that the components of the signal at nodes i and j exert on one another. Examples of GSOs include the adjacency matrix [29], the Laplacian matrix [30], the random walk matrix [31] and their normalizations. By construction, the GSO can be used to define $\mathbf{S}\mathbf{x}$ as the elementary linear and local map between graph signals. We say that this map is local because the i th

entry of the output, $[\mathbf{S}\mathbf{x}]_i$, is a linear combination of the signal components in the one-hop neighborhood of i . Explicitly,

$$[\mathbf{S}\mathbf{x}]_i = \sum_{j=1}^N [\mathbf{S}]_{ij} [\mathbf{x}]_j = \sum_{j \in \mathcal{N}_i} s_{ij} x_j. \quad (3)$$

where $\mathcal{N}_i = \{j \in \mathcal{N} : (j, i) \in \mathcal{E}\}$ denotes the set of immediate neighbors of i . The second equality follows from the fact that $[\mathbf{S}]_{ij} = 0$ for all $j \notin \mathcal{N}_i$. In a sense, we can view the operation $\mathbf{S}\mathbf{x}$ as a shift (or diffusion) of the signal on the graph, where the value of the signal at each node is updated as a linear combination of signal values at neighboring nodes.

The notion of *graph shifts* can be used to define *graph convolutions* analogous to *time convolutions*. Formally, we define the graph convolution as a weighted sum of shifted versions of the signal [19], [32],

$$\mathbf{A}(\mathbf{S})\mathbf{x} = \sum_{k=0}^{K-1} a_k \mathbf{S}^k \mathbf{x}. \quad (4)$$

Note that, since $\mathbf{S}^k \mathbf{x} = \mathbf{S}(\mathbf{S}^{k-1} \mathbf{x})$, repeated applications of the linear map \mathbf{S} entail successive exchanges with neighboring nodes; this means that the graph convolution can be computed as a series of local operations. Also note that the operation $\mathbf{S}^k \mathbf{x}$ produces a summary of the information contained in the k -hop neighborhood of each node. For $0 \leq k \leq K-1$, the filter *coefficients* (or filter *taps*) $\mathbf{a} = [a_0, a_1, \dots, a_{K-1}] \in \mathbb{R}^K$ assign different importances to the information located in each k -hop neighborhood. Following the graph signal processing terminology, $\mathbf{A}(\mathbf{S}) \in \mathbb{R}^{N \times N}$ is called a *linear shift-invariant graph filter* (LSI-GF) [33], which reinforces the analogy with time-invariant filters and the convolution operation.

In what follows, the data sequences that we consider will be *graph processes*. A graph process is a sequence $\{\mathbf{x}_t\}_{t \in \mathbb{N}_0}$ of signals $\mathbf{x}_t \in \mathbb{R}^N$ supported on the graph \mathcal{G} . Alternatively, a graph process can also be seen as a time-varying graph signal where the values of the signal at each node change over time [34], [35]. While traditional RNNs (Section II-A) successfully exploit the sequential structure of data, they fail to account for other structures that may be present in \mathbf{x}_t ; however, as substantiated by the remarkable performance achieved by CNNs [7]–[9] and GNNs [10]–[12], exploiting the data's *spatial* structure is of paramount importance. The first contribution of this paper is thus to adapt RNNs to exploit the underlying structure of graph signals.

III. GRAPH RECURRENT NEURAL NETWORKS

As previously noted in Section II-A, RNNs exploit the HMM model approximation to devise a *learning* framework capable of learning causal dependencies in sequences of variable length, with a number of parameters that is independent of time. However, the number of parameters still depends on the dimension N , which not only prevents RNNs from scaling to inputs with large dimensions but, more importantly, hinders their ability to account for other inherent structures of data. Accounting for structure is desirable first, because when we parametrize operations in terms of the structure of the data, we are effectively adding a constraint to the optimization

problem, shrinking the feasible set and making it easier to find close-to-optimal solutions; and, second, because it allows us to leverage repeating and/or symmetrical motifs in the data to extract shared features and simplify model parametrization. In the case of graph processes, we will thus adapt the operations performed by RNNs to take the graph structure into account. We assume that the hidden state $\mathbf{z}_t \in \mathbb{R}^N$ is itself a graph signal, so that each entry $[\mathbf{z}_t]_n$ is a *nodal* hidden state. The updated hidden state can then be calculated by parametrizing the linear maps \mathbf{A} and \mathbf{B} by the graph shift operator \mathbf{S} , yielding

$$\mathbf{z}_t = \sigma(\mathbf{A}(\mathbf{S})\mathbf{x}_t + \mathbf{B}(\mathbf{S})\mathbf{z}_{t-1}). \quad (5)$$

We call this architecture the *graph recurrent neural network* (GRNN). Although $\mathbf{A}(\mathbf{S})$ and $\mathbf{B}(\mathbf{S})$ can be arbitrary functions of \mathbf{S} [36], we opt for the graph convolution, (4) so that there are only K parameters to learn for each filter ($\mathbf{a} = [a_0, \dots, a_{K-1}] \in \mathbb{R}^K$ and $\mathbf{b} = [b_0, \dots, b_{K-1}] \in \mathbb{R}^K$). This allows computations to be done locally and, like in GNNs, ensures that the number of parameters is independent of the size of the graph. Other advantages of graph convolutions are that they are permutation equivariant and stable to graph perturbations [21], a fact that we use to derive a stability result for GRNNs in Section IV.

To estimate the target representation \mathcal{Y} , we can once again leverage the fact that the hidden state \mathbf{z}_t is a graph signal and use a GNN $\Phi(\mathbf{z}_t; \mathbf{S})$ [12] to compute the estimate $\hat{\mathcal{Y}}$. In cases where \mathbf{y}_t is itself a graph signal (e.g., in regression or forecasting), Φ can be a simple one-layer graph filter followed by an activation function ρ ,

$$\hat{\mathbf{y}}_t = \rho(\mathbf{C}(\mathbf{S})\mathbf{z}_t) \quad (6)$$

where we parametrize the filter $\mathbf{C}(\mathbf{S})$ as a graph convolution (4) with K filter taps ($\mathbf{c} \in \mathbb{R}^K$) to make sure that the number of parameters of the entire architecture (5)–(6) is completely independent of the size of the graph. If \mathbf{y}_t has dimension $M \neq N$ then $\mathbf{C}(\mathbf{S})$ must be followed by an additional operation mapping N dimensions to M dimensions (a fully connected layer –perceptron–, for instance), in which case the number of parameters of $\mathbf{C}(\mathbf{S})$ will necessarily depend on N and M . Finally, if \mathbf{y}_t is single value y representing the entire sequence $\{\mathbf{x}_t\}_{t=1}^T$, we compute it from the last state alone as $\hat{y} = \rho(\mathbf{C}(\mathbf{S})\mathbf{z}_T)$.

Making the hidden state \mathbf{z}_t a graph signal has several advantages. First, it adds interpretability to the value of this signal with respect to the underlying graph support. For instance, we could analyze the frequency content of the hidden state and compare it with the frequency content of the graph process \mathbf{x}_t . Second, it allows the computation of \mathbf{z}_t to be done in an entirely local fashion, involving only repeated exchanges with the one-hop neighbors of each node. Making \mathbf{z}_t a graph signal, however, also implies that we can no longer tune the size of the hidden state which is now fixed at N . The size of the hidden state is a fundamental hyperparameter in the design of RNNs since it controls the description capability of the HMM. This can be overcome by introducing graph signal tensors where, instead of a single scalar, a vector of features is assigned to each node.

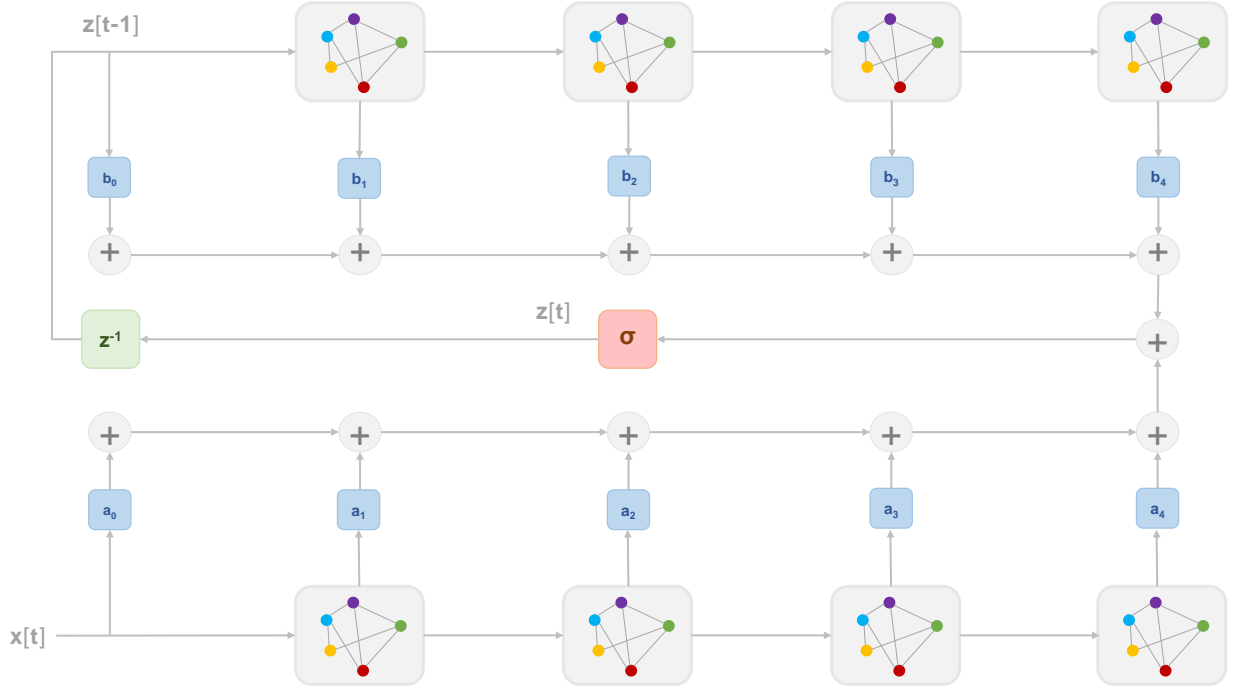


Figure 1. State computation in a graph recurrent neural network with $K = 5$. Gray blocks with graphs on the inside stand for graph shifts, blue blocks for linear weights, the red block for a pointwise nonlinearity and the green block for a time delay.

A graph signal tensor is a function $\mathbf{X} : \mathcal{V} \rightarrow \mathbb{R}^F$ that assigns a vector of dimension F to each node. Each entry of this vector is a *feature*. The signal tensor can be represented as a $N \times F$ matrix \mathbf{X} , where each column $\mathbf{x}^f \in \mathbb{R}^N$ is a graph signal corresponding to the values of feature f across all nodes.

The graph convolution operation (4) must be extended accordingly, so as to carry out a local, linear transformation mapping the F input features in $\mathbf{X} \in \mathbb{R}^{N \times F}$ to the G output features $\mathbf{Y} \in \mathbb{R}^{N \times G}$. This map is implemented by a bank of FG graph filters of order K , with filter taps given by $\mathbf{a}^{fg} = [a_0^{fg}, \dots, a_{K-1}^{fg}]$. The graph convolution $\mathcal{A}_S : \mathbb{R}^{N \times F} \rightarrow \mathbb{R}^{N \times G}$ becomes [cf. (4)],

$$\mathbf{Y} = \mathcal{A}_S(\mathbf{X}) = \sum_{k=0}^{K-1} \mathbf{S}^k \mathbf{X} \mathbf{A}_k \quad (7)$$

where $\mathbf{A}_k \in \mathbb{R}^{F \times G}$ is a matrix satisfying $[\mathbf{A}_k]_{fg} = a_k^{fg}$. We can see that, for the convolution to be local on the graph, the operations that modify \mathbf{X} on the left have to respect the sparsity of the graph, while those that modify it on the right can be arbitrary linear operations. The right operations have the role of mixing the features within a single node, using the same linear combination –parameter sharing– across all nodes.

Given a sequence of graph signal tensors $\{\mathbf{X}_t\}$, $\mathbf{X}_t \in \mathbb{R}^{N \times F}$, we can rewrite equation (5) to obtain H -feature hidden state tensors $\mathbf{Z}_t \in \mathbb{R}^{N \times H}$,

$$\mathbf{Z}_t = \sigma \left(\mathcal{A}_S(\mathbf{X}_t) + \mathcal{B}_S(\mathbf{Z}_{t-1}) \right) \quad (8)$$

where the filter taps are $\mathbf{A}_k \in \mathbb{R}^{F \times H}$ and $\mathbf{B}_k \in \mathbb{R}^{H \times H}$, $k = 0, \dots, K-1$. Assuming that the target representation is also

a graph signal tensor, it can be generalized as $\mathbf{Y}_t \in \mathbb{R}^{Y \times G}$, which we calculate as

$$\mathbf{Y}_t = \rho \left(\mathcal{C}_S(\mathbf{Z}_t) \right) \quad (9)$$

with filter taps $\mathbf{C}_k \in \mathbb{R}^{G \times H}$, $k = 0, \dots, K-1$.

By using graph signal tensors to describe the hidden state, we retrieve the ability to tune its descriptive power through the value of H . Additionally, note that the output \mathbf{Y}_t can be computed straight from the individual hidden state feature values at each node, minimizing the communication cost. To achieve this, it suffices to make \mathcal{C}_S a graph convolution (7) with $K = 1$, in which case no neighborhood exchanges take place. This architecture only requires node communications at updates of the hidden state \mathbf{Z}_t .

IV. STABILITY OF GRNNs

The performance of GRNNs (and of graph filters in general) depends on the underlying graph support. If the graph changes, or is not estimated accurately, the output of the GRNN can be different than expected. In what follows, we obtain an upper bound on the changes at the output of a GRNN caused by perturbations in the underlying graph. We use this result to quantify how *adaptable* GRNNs are to time-varying scenarios and transfer learning [37]. We focus on single-feature GRNNs (5)-(6) for simplicity, but results for the multi-feature case carry out similarly [21].

Let \mathbf{S} be the GSO of a given graph, and let $\tilde{\mathbf{S}}$ be the GSO of the graph resulting from a perturbation of this graph. Let

us first consider the case of node relabelings, in which $\tilde{\mathbf{S}} = \mathbf{P}^\top \mathbf{S} \mathbf{P}$. The matrix \mathbf{P} is a permutation matrix $\mathbf{P} \in \mathcal{P}$ with

$$\mathcal{P} = \{\mathbf{P} \in \{0, 1\}^{N \times N} : \mathbf{P}\mathbf{1} = \mathbf{1}, \mathbf{P}^\top \mathbf{1} = \mathbf{1}\}. \quad (10)$$

If the perturbed graph is simply a permutation of the original graph, then the output of the GRNN running on the permuted graph is the permutation of the output of the GRNN running on the original graph.

Proposition 1. Let \mathbf{S} be a GSO and $\tilde{\mathbf{S}} = \mathbf{P}^\top \mathbf{S} \mathbf{P}$ be a permutation of this GSO, for some permutation matrix $\mathbf{P} \in \mathcal{P}$. Let \mathbf{x}_t be a graph signal and $\tilde{\mathbf{x}}_t = \mathbf{P}^\top \mathbf{x}_t$ the permuted version of the signal. Then, it holds that

$$\tilde{\mathbf{z}}_t = \sigma(\mathbf{A}(\tilde{\mathbf{S}})\tilde{\mathbf{x}}_t + \mathbf{B}(\tilde{\mathbf{S}})\tilde{\mathbf{z}}_{t-1}) = \mathbf{P}^\top \mathbf{z}_t \quad (11)$$

$$\tilde{\mathbf{y}}_t = \rho(\mathbf{C}(\tilde{\mathbf{S}})\tilde{\mathbf{z}}_t) = \mathbf{P}^\top \mathbf{y}_t \quad (12)$$

for all t .

Proof. Refer to Appendix A. \square

Proposition 1 states that GRNNs are independent of any chosen node labeling. Note that this result holds irrespective of whether we know the value of \mathbf{P} or not. It also indicates that GRNNs are able to exploit the internal symmetries of graph processes in the course of learning. This means that by learning how to process a signal on a given part of the graph, GRNNs are also learning to process it in all other parts of the graph that are topologically symmetric. The permutation equivariance property can thus be seen as an implicit mechanism of *data augmentation*.

When considering more general perturbations $\tilde{\mathbf{S}} \in \mathbb{R}^{N \times N}$, Proposition 1 suggests that distances should be measured modulo permutations. In order to do so, we introduce the notion of relative perturbation in Definition 1.

Definition 1 (Relative perturbation matrices). Given GSOs \mathbf{S} and $\tilde{\mathbf{S}}$, we define the set of relative perturbation matrices modulo permutation as

$$\mathcal{E}(\mathbf{S}, \tilde{\mathbf{S}}) = \left\{ \mathbf{E} \in \mathbb{R}^{N \times N} : \mathbf{P}^\top \tilde{\mathbf{S}} \mathbf{P} = \mathbf{S} + \mathbf{E} \mathbf{S} + \mathbf{S} \mathbf{E}^\top, \mathbf{P} \in \mathcal{P} \right\}. \quad (13)$$

We define the distance between two graphs described by \mathbf{S} and $\tilde{\mathbf{S}}$ respectively as

$$d(\mathbf{S}, \tilde{\mathbf{S}}) = \min_{\mathbf{E} \in \mathcal{E}(\mathbf{S}, \tilde{\mathbf{S}})} \|\mathbf{E}\|. \quad (14)$$

Notice that if $\tilde{\mathbf{S}}$ is a permutation of \mathbf{S} , then $d(\mathbf{S}, \tilde{\mathbf{S}}) = 0$ as expected.

To understand the effect of graph perturbations on the output of GRNNs, we first look at their effect on graph convolutions (4). In particular, we leverage the graph Fourier transform (GFT) [38] to analyze the spectral representations of the convolved graph signals. Let $\mathbf{S} = \mathbf{V} \mathbf{\Lambda} \mathbf{V}^\top$ be the eigendecomposition of the GSO \mathbf{S} , where $\mathbf{V} = [\mathbf{v}_1, \dots, \mathbf{v}_N]$ is the orthogonal matrix of eigenvectors, and $\mathbf{\Lambda} = \text{diag}(\lambda_1, \dots, \lambda_N)$ is the diagonal matrix of eigenvalues λ_n . The GFT of a signal is computed by projecting the signal on the graph's eigenvector

basis. The GFT of the output of a convolved graph signal is thus

$$\mathbf{V}^\top \mathbf{A}(\mathbf{S}) \mathbf{x} = \mathbf{V}^\top \sum_{k=0}^{K-1} a_k \mathbf{V} \mathbf{\Lambda}^k \mathbf{V}^\top \mathbf{x} = \mathbf{A}(\mathbf{\Lambda}) (\mathbf{V}^\top \mathbf{x}) \quad (15)$$

where $\mathbf{A}(\mathbf{\Lambda})$ is a diagonal matrix such that $[\mathbf{A}(\mathbf{\Lambda})]_n = \sum_{k=0}^{K-1} a_k \lambda_n^k = a(\lambda_n)$. We refer to the function $a(\lambda)$ as the *frequency response* of the filter,

$$a(\lambda) = \sum_{k=0}^{K-1} a_k \lambda^k. \quad (16)$$

For a given graph, this frequency response gets instantiated on the graph's eigenvalues $\{\lambda_n\}$ as $\mathbf{A}(\mathbf{\Lambda})$, determining the specific effect that the filter has on the input due to the underlying support (15). Note, however, that the general expression of the frequency response (16) only depends on the filter taps $\{a_k\}$, which are independent of the graph.

The results here derived are for graph filters with *integral Lipschitz* frequency response.

Definition 2 (Integral Lipschitz filters). Given a set of filter taps $\{a_k\}$, we say that the filter $\mathbf{A}(\mathbf{S})$ [cf. (4)] is integral Lipschitz if its frequency response $a(\lambda)$ [cf. (16)] satisfies

$$|a(\lambda_2) - a(\lambda_1)| \leq C \frac{|\lambda_2 - \lambda_1|}{|\lambda_1 + \lambda_2|/2} \quad (17)$$

for all $C > 0$ and all $\lambda_1, \lambda_2 \in \mathbb{R}$.

We note that integral Lipschitz filters also satisfy $|\lambda a'(\lambda)| \leq C$, where $a'(\lambda)$ is the derivative of $a(\lambda)$. This condition is reminiscent of the scale invariance of wavelet transforms [39, Chapter 7].

In the following, we prove that GRNNs built from integral Lipschitz filters are stable under relative perturbations.

Theorem 1. Let $\mathbf{S} = \mathbf{V} \mathbf{\Lambda} \mathbf{V}^\top$ and $\tilde{\mathbf{S}}$ represent graphs with N nodes. Let $\mathbf{E} = \mathbf{U} \mathbf{M} \mathbf{U}^\top \in \mathcal{E}(\mathbf{S}, \tilde{\mathbf{S}})$ be a relative perturbation matrix [cf. (13)] such that [cf. (14)]

$$d(\mathbf{S}, \tilde{\mathbf{S}}) \leq \|\mathbf{E}\| \leq \varepsilon. \quad (18)$$

Consider a GRNN (5)-(6) with integral Lipschitz filters \mathbf{A} , \mathbf{B} and \mathbf{C} with constants C_A , C_B and C_C and normalized filter height $\|\mathbf{A}\| = \|\mathbf{B}\| = \|\mathbf{C}\| = 1$, respectively [cf. (17)]. Consider pointwise nonlinearities σ, ρ that are normalized Lipschitz, $|\sigma(b) - \sigma(a)| \leq |b - a|$ for all $a, b \in \mathbb{R}$, and that satisfy $\sigma(0) = 0$. Let $\mathbf{z}_0 = \mathbf{0}$ and $\|\mathbf{x}_t\| \leq \|\mathbf{x}\| = 1$ for every t . Then, it holds that

$$\min_{\mathbf{P} \in \mathcal{P}} \|\mathbf{y}_t - \mathbf{P}^\top \tilde{\mathbf{y}}_t\| \leq C(1 + \sqrt{N}\delta)(t^2 + 3t)\varepsilon + \mathcal{O}(\varepsilon^2) \quad (19)$$

where \mathbf{y}_t is the output of the GRNN running on \mathbf{S} and $\tilde{\mathbf{y}}_t$ is the output of the one running on $\tilde{\mathbf{S}}$. The constant C denotes the maximum filter constant, $C = \max\{C_A, C_B, C_C\}$, and $\delta = (\|\mathbf{U} - \mathbf{V}\| + 1)^2 - 1$ measures the eigenvector misalignment between the GSO \mathbf{S} and the error matrix \mathbf{E} .

Proof. Refer to Appendix B. \square

Theorem 1 states that, for a graph process of length $t = T$, the output of a GRNN is Lipschitz stable to relative graph

perturbations [cf. Def. 1] with constant $C(1+\sqrt{N}\delta)(T^2+3T)$. We see that the stability of a GRNN depends on the Lipschitz filter constant C . This is a *design* parameter that, while it could be set at a fixed value, it is usually learned from data through the filter taps of \mathbf{A} , \mathbf{B} and \mathbf{C} . The term $(1+\delta\sqrt{N})$ measures the eigenvector misalignment and is a property of the graph perturbation. Unlike C , it cannot be controlled by design. Finally, the stability of GRNNs depends polynomially on the length T of the process, with T^2+3T . The linear term arises from sequential applications of the filters \mathbf{A} , \mathbf{B} and \mathbf{C} , and the square term is a result of the recurrence on \mathbf{z}_t . While T can be controlled by restraining the length of the graph processes that we consider (or by splitting them in multiple shorter processes), this affects the architecture's ability to learn long-term dependencies. Thus, there exists a trade-off between the length of the sequence and the stability of the architecture. One way to control this trade-off is by carefully designing \mathbf{A} , \mathbf{B} and \mathbf{C} . As explained in the next section, the instabilities associated with long sequences can also be mitigated through gating.

V. GATED GRNN ARCHITECTURES

Traditional RNN architectures suffer from the problem of *vanishing (exploding) gradients* when the input sequence contains long term dependencies [40], [41]. The same holds for GRNNs when the eigenvalues of $\mathbf{B}(\mathbf{S})$ are smaller (or larger) than 1. Long term dependencies can also be an issue from a stability standpoint, as the stability constant derived in Theorem 1 depends polynomially on t . RNN architectures typically address problems associated with long term dependencies by the addition of time gating mechanisms [16, Chapter 10], which can be naturally extended to GRNNs (Sec. V-A).

When dealing with graph processes, we may also encounter what we call the problem of *vanishing gradients in space* (in contrast with the aforementioned problem of *vanishing gradients in time*). Even if the eigenvalues of $\mathbf{B}(\mathbf{S})$ are well-behaved, some nodes or paths of the graph might get assigned more importance than others in long range exchanges, leading to *spatial imbalances* that make it challenging to encode certain graph spatial dependencies. This problem can be explained by the fact that the matrix multiplications by $\mathbf{B}(\mathbf{S})$ are actually multiplications by powers of \mathbf{S} . As an example, consider a graph where some components have higher connectivities than others. For large t , the matrix entries associated with the nodes belonging to highly connected components will get densely populated, overshadowing other local, sparser structures of these components and making it harder to distinguish long range processes that are local on the graph.

To attenuate these issues, we propose to add a more comprehensive *gating mechanism* to GRNNs. Similarly to the gates employed in traditional RNNs, the gates that we consider are operators acting on the current input and previous state to control how much of the input should be taken into account and how much past information should be *remembered* (or *forgotten*) in the computation of the new state. These gating operators are updated at every step of the sequence and, as such, they are able to create multiple dependency paths

between states and inputs in both time and space. This allows for both short and long term dependencies to be encoded by the model without getting assigned exponentially smaller or larger weights. Adding gating to GRNNs yields the Gated GRNN (GGRNN), in which \mathbf{Z}_t is computed as

$$\mathbf{Z}_t = \sigma \left(\hat{\mathcal{Q}} \{ \mathcal{A}_S(\mathbf{X}_t) \} + \check{\mathcal{Q}} \{ \mathcal{B}_S(\mathbf{Z}_{t-1}) \} \right) \quad (20)$$

and where $\hat{\mathcal{Q}} : \mathbb{R}^{N \times H} \rightarrow \mathbb{R}^{N \times H}$ stands for the *input gate* operator and $\check{\mathcal{Q}} : \mathbb{R}^{N \times H} \rightarrow \mathbb{R}^{N \times H}$ for the *forget gate* operator.

Depending on the choice of gating strategy, which we will discuss in the following subsections, $\hat{\mathcal{Q}}$ and $\check{\mathcal{Q}}$ take on different forms. What they all have in common is that their parameters are themselves calculated as the output of GRNNs. The GRNN used to calculate the input gate has *input gate state* $\hat{\mathbf{Z}}_t \in \mathbb{R}^{N \times \hat{H}}$ given by

$$\hat{\mathbf{Z}}_t = \hat{\sigma} \left(\hat{\mathcal{A}}_S(\mathbf{X}_t) + \hat{\mathcal{B}}_S(\hat{\mathbf{Z}}_{t-1}) \right) \quad (21)$$

and the GRNN used to calculate the forget gate has *forget gate state* $\check{\mathbf{Z}}_t \in \mathbb{R}^{N \times \check{H}}$,

$$\check{\mathbf{Z}}_t = \check{\sigma} \left(\check{\mathcal{A}}_S(\mathbf{X}_t) + \check{\mathcal{B}}_S(\check{\mathbf{Z}}_{t-1}) \right) \quad (22)$$

where $\hat{\mathcal{A}}_S$, $\hat{\mathcal{B}}_S$, $\check{\mathcal{A}}_S$ and $\check{\mathcal{B}}_S$ are graph convolutions [cf. (7)] with filter taps $\hat{\mathbf{A}}_k \in \mathbb{R}^{F \times \hat{H}}$, $\hat{\mathbf{B}}_k \in \mathbb{R}^{\hat{H} \times \hat{H}}$, $\check{\mathbf{A}}_k \in \mathbb{R}^{F \times \check{H}}$ and $\check{\mathbf{B}}_k \in \mathbb{R}^{\check{H} \times \check{H}}$.

To tackle the different time and spatial imbalance scenarios described in this section, we envision three gating strategies: time (Sec. V-A), node (Sec. V-B) and edge gating (Sec. V-C).

A. Time gating

In the *Time Gated GRNN* (t-GGRNN), the input and forget gate operators $\hat{\mathcal{Q}}$ and $\check{\mathcal{Q}}$ take form

$$\begin{aligned} \hat{\mathcal{Q}} \{ \mathcal{A}_S(\mathbf{X}_t) \} &= \hat{q}_t \mathcal{A}_S(\mathbf{X}_t) \\ \check{\mathcal{Q}} \{ \mathcal{B}_S(\mathbf{Z}_t) \} &= \check{q}_t \mathcal{B}_S(\mathbf{Z}_t) \end{aligned} \quad (23)$$

with $\hat{q}_t \in [0, 1]$ and $\check{q}_t \in [0, 1]$ computed as

$$\begin{aligned} \hat{q}_t &= \text{sigmoid}(\hat{\mathbf{c}}^T \text{vec}(\hat{\mathbf{Z}}_t)) \\ \check{q}_t &= \text{sigmoid}(\check{\mathbf{c}}^T \text{vec}(\check{\mathbf{Z}}_t)) \end{aligned} \quad (24)$$

and where $\hat{\mathbf{c}} \in \mathbb{R}^{\hat{H}N}$ and $\check{\mathbf{c}} \in \mathbb{R}^{\check{H}N}$ are the learnable parameters.

Time gating addresses the problem of vanishing gradients in time by learning scalar gates between 0 and 1 and multiplying the input and state variables by these gates, thus compensating for imbalanced gradient paths associated with eigenvalues that are too small or too large. We refer to this strategy as time gating because it only acts on time dependencies, *shutting down* the whole input and/or the whole previous state at each time instant as needed, without discriminating between nodes. Here, note that the number of parameters necessary to map the state to the input and forget gates are dependent on the size of the graph, because all of the graph signal components must be mapped onto scalar variables.

The basic architecture of a t-GGRNN resembles that of the Long Short-Term Memory units (LSTMs) used to process

regular data sequences [16, Chapter 10], with the difference that LSTMs have an output gate in addition to the input and forget gates. The input and forget gates of a LSTM are calculated in the same way \hat{q}_t and \check{q}_t in (24) would be if we considered the directed cycle graph. Another common gated architecture for regular data are Gated Recurrent Units (GRUs) [16, Chapter 10], which are even simpler than LSTMs where only one gating variable $u_t \in [0, 1]$ acts as the forget gate of LSTMs, and where the input gate is replaced by $1 - u_t$. The GRU architecture can be readily extended to t-GGRNNs.

B. Node gating

In some cases, having the input and forget gates of a gated GRNN be scalars is limiting because the short/long term time interactions of the graph process might vary across nodes. This is especially true of graph processes that are, in reality, some unknown composition of processes happening independently at each node and/or on multiple, possibly non-disjoint, subgraphs of the original graph. In the Node Gated GRNN (n-GGRNN), we address this by defining the input gate and forget gate operators \hat{Q} and \check{Q} as

$$\begin{aligned}\hat{Q}\{\mathcal{A}_S(\mathbf{X}_t)\} &= \text{diag}(\hat{\mathbf{q}}_t)\mathcal{A}_S(\mathbf{X}_t) \\ \check{Q}\{\mathcal{B}_S(\mathbf{Z}_t)\} &= \text{diag}(\check{\mathbf{q}}_t)\mathcal{B}_S(\mathbf{Z}_t)\end{aligned}\quad (25)$$

with vector parameters $\hat{\mathbf{q}}_t \in [0, 1]^N$ and $\check{\mathbf{q}}_t \in [0, 1]^N$ calculated as

$$\begin{aligned}\hat{\mathbf{q}}_t &= \text{sigmoid}(\hat{\mathbf{C}}_S(\hat{\mathbf{Z}}_t)) \\ \check{\mathbf{q}}_t &= \text{sigmoid}(\check{\mathbf{C}}_S(\check{\mathbf{Z}}_t))\end{aligned}\quad (26)$$

and where, now, the learnable parameters are the filter taps of the graph convolutions $\hat{\mathbf{C}}_S$ and $\check{\mathbf{C}}_S$, given by $\hat{\mathbf{C}}_k \in \mathbb{R}^{1 \times \hat{H}}$ and $\check{\mathbf{C}}_k \in \mathbb{R}^{1 \times \check{H}}$.

In the n-GGRNN, the gates $\hat{\mathbf{q}}_t$ and $\check{\mathbf{q}}_t$ are reshaped as the diagonal matrices $\text{diag}(\hat{\mathbf{q}}_t)$ and $\text{diag}(\check{\mathbf{q}}_t)$, which then multiply the input and state variables. The multiplication by $\text{diag}(\hat{\mathbf{q}}_t)$ and $\text{diag}(\check{\mathbf{q}}_t)$ has the role of applying a separate scalar input and forget gate (both taking values between 0 and 1) to each node. This allows addressing the problem of vanishing gradients in space by controlling the importance of the input and of the state at the node level and partially shutting down nodes whose signal components can effectively behave as noise in the exchanges involved in some learning tasks. Besides adding flexibility to the gated architecture, n-GGRNNs have the advantage that their number of parameters is independent of the size of the graph, which could not be said about the t-GGRNNs from the previous subsection.

An interesting observation is that the composition of node gating with a graph convolution can be interpreted as the application of a node-varying graph filter [42], which, instead of weighing powers of \mathbf{S} by scalars as in the LSI-GF (cf. (4)), multiplies them by diagonal matrices assigning a different weight to each node. From an implementation standpoint, this is important because it allows simplifying the operations involved in the n-GGRNN.

C. Edge gating

In node gating, we control long range graph dependencies by assigning a gate to each node *after* local exchanges have occurred. In edge gating, the gates act within these local exchanges, controlling the amount of information that is transmitted across edges of the graph. The input and forget gate operators take form

$$\begin{aligned}\hat{Q}\{\mathcal{A}_S(\mathbf{X}_t)\} &= \mathcal{A}_{\mathbf{S} \odot \hat{\mathbf{Q}}_t}(\mathbf{X}_t) \\ \check{Q}\{\mathcal{B}_S(\mathbf{Z}_t)\} &= \mathcal{B}_{\mathbf{S} \odot \check{\mathbf{Q}}_t}(\mathbf{Z}_t)\end{aligned}\quad (27)$$

where the shift operators that parametrize the input-to-state and state-to-state convolutions are now $\mathbf{S} \odot \hat{\mathbf{Q}}_t$ and $\mathbf{S} \odot \check{\mathbf{Q}}_t$ respectively, with $\hat{\mathbf{Q}}_t, \check{\mathbf{Q}}_t \in [0, 1]^{N \times N}$. $\hat{\mathbf{Q}}_t$ and $\check{\mathbf{Q}}_t$ are calculated as

$$\begin{aligned}[\hat{\mathbf{Q}}_t]_{ij} &= \text{sigmoid}(\hat{\mathbf{c}}^\top [\delta_i^\top \hat{\mathbf{Z}}_t \hat{\mathbf{C}} \parallel \delta_j^\top \hat{\mathbf{Z}}_t \hat{\mathbf{C}}]^\top) \\ [\check{\mathbf{Q}}_t]_{ij} &= \text{sigmoid}(\check{\mathbf{c}}^\top [\delta_i^\top \check{\mathbf{Z}}_t \check{\mathbf{C}} \parallel \delta_j^\top \check{\mathbf{Z}}_t \check{\mathbf{C}}]^\top)\end{aligned}\quad (28)$$

where δ_i stands for the one-hot column vector with $[\delta_i]_i = 1$ and \parallel is the horizontal concatenation operation. The learnable parameters are $\hat{\mathbf{C}} \in \mathbb{R}^{\hat{H} \times \hat{H}'}$, $\hat{\mathbf{c}} \in \mathbb{R}^{2\hat{H}' \times 1}$, $\check{\mathbf{C}} \in \mathbb{R}^{\check{H} \times \check{H}'}$ and $\check{\mathbf{c}} \in \mathbb{R}^{2\check{H}' \times 1}$, and \hat{H}' and \check{H}' are arbitrary numbers of *intermediate* features.

Effectively, $\hat{\mathbf{Q}}_t$ and $\check{\mathbf{Q}}_t$ scale the weight of each edge by a value between 0 and 1. When this value is 0, the edge exchange is completely shut off, which can be helpful in GRNNs running on graphs with noisy or spurious edges, e.g. graphs built from sample covariance matrices. Note that each edge input gate $[\hat{\mathbf{Q}}_t]_{ij}$ and forget gate $[\check{\mathbf{Q}}_t]_{ij}$ is computed individually, avoiding unnecessary computations for pairs (i, j) that do not correspond to edges of the graph.

In practice, in our architecture the computations carried out in equation (28) are implemented as Graph Attention Networks (GAN) [43], whose *attention coefficients* play the role of $[\hat{\mathbf{Q}}_t]_{ij}$ and $[\check{\mathbf{Q}}_t]_{ij}$. Specifically tailored to graphs, GATs are attention mechanisms that generate meaningful representations of graph signals by incorporating the importance of a node's features to its neighbors in the extraction of subsequent features. This importance is learned in the form of attention coefficients between nodes i and j that are connected by an edge, and is calculated by applying a linear transformation and a nonlinearity to the concatenated features of i and j . Following normalization (either by a nonlinearity such as the sigmoid or by some other normalizing operation), the attention coefficients of GATs taking in $\hat{\mathbf{Z}}_t$ and $\check{\mathbf{Z}}_t$ are well-suited implementations of the input and forget edge gates $[\hat{\mathbf{Q}}_t]_{ij}$ and $[\check{\mathbf{Q}}_t]_{ij}$.

Similarly to how the composition of node gating with a graph convolution could be interpreted as a node-varying graph filter, composing edge gating with LSI-GFs can be seen as a particular implementation of an edge-varying graph filter [36], [44], [45]. Edge-varying graph filters are such that each edge is parametrized independently in multiplications by the GSO, which is precisely what happens when edge gates are applied to \mathbf{S} in the input-to-state and state-to-state convolutions.

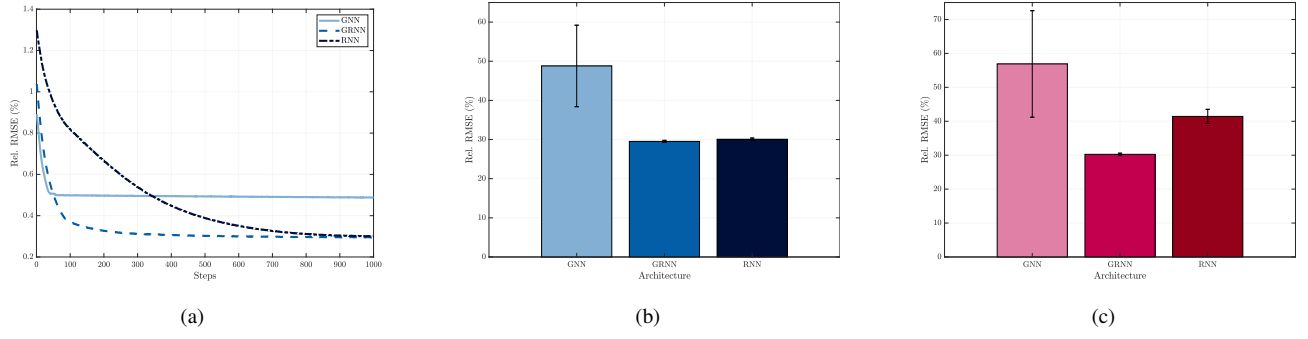


Figure 2. 5-step prediction using a GNN, a GRNN and a RNN. (a) Training rRMSE evolution over 1000 training steps. (b) Average test rRMSEs for 5 graphs and 5 data realizations, using a 10,000-sample training dataset. (c) Average test rRMSEs for 5 graphs and 5 data realizations, using a 5,000-sample training dataset.

VI. NUMERICAL EXPERIMENTS

In this section, we present a series of numerical experiments where the GRNN is compared with GNNs and RNNs, and where the advantages of time, node and edge gating are analyzed. In the first four experiments (subsections VI-A, VI-B, VI-C, VI-D), we use synthetic data to simulate the problem of k -step prediction, where, given instantaneous observations of a synthetic graph process, the objective is to predict the graph signals observed k steps ahead. In each subsection, a different type of process is considered to assess the advantages of various gating strategies in different scenarios. The fifth experiment (subsection VI-E) uses earthquake data from New Zealand's Geonet database [46] to predict the region of origin of each earthquake registered between June 17, 2019 and July 17, 2019. This data consists of 10s and 20s seismograph readings measured on a network of $N = 59$ seismographs immediately before each earthquake, and all earthquakes are assigned a class label corresponding to one out of $C = 11$ regions.

In the k -step prediction experiments (subsections VI-A, VI-B, VI-C, VI-D), we optimize the mean absolute error (MAE), or L1 loss, to train the model, and evaluate its performance in terms of the relative root mean square error (rRMSE). In the earthquake epicenter estimation experiment (subsection VI-E), we optimize the cross-entropy loss and evaluate classification accuracy.

All recurrent architectures have a single recurrent layer, the state nonlinearity σ is always the tanh function and the nonlinearities of the GNNs with which we compare our architectures are ReLUs. All models are trained using the ADAM algorithm [47] with decaying factors $\beta_1 = 0.9$ and $\beta_2 = 0.999$. We will denote the number of input features by F_X and the number of state features by F_Z ; the number of filter taps in \mathcal{A}_S and \mathcal{B}_S are K_X and K_Z respectively. When \mathcal{C}_S is a multi-layer GNN, or when we are comparing against a GNN architecture, the number of features produced by layer ℓ of the GNN is F_ℓ , and the number of filter taps of this layer is K_ℓ . When applicable, the number of output features will be denoted by F_Y .

A. k -step prediction: GRNN vs. GNN vs. RNN

Let \mathcal{G} be an SBM graph with $N = 80$ nodes, $c = 5$ communities, intra-community probability $p_{c_i c_i} = 0.8$ and inter-community probability $p_{c_i c_j} = 0.2$. We write a noisy diffusion process on this graph as

$$\mathbf{x}_t = \mathbf{S}\mathbf{x}_{t-1} + \mathbf{w}_t \quad (29)$$

where $\mathbf{x}_t \in \mathbb{R}^N$ is a graph signal, $\mathbf{S} \in \mathbb{R}^{N \times N}$ is the GSO and $\mathbf{w}_t \in \mathbb{R}^N$ is a zero-mean Gaussian noise with temporal variance $\xi^2 = 0.01$ and spatial variance (across nodes) $\eta^2 = 0.01$. The problem of k -step prediction consists of estimating $\mathbf{x}_{t+k}, \mathbf{x}_{t+k+1}, \mathbf{x}_{t+k+2}, \dots$ from $\mathbf{x}_t, \mathbf{x}_{t+1}, \mathbf{x}_{t+2}, \dots$

We simulate this process for many values of \mathbf{x}_0 and over multiple time steps, feeding the generated data to three neural network models trained to predict the diffused graph signals $k = 5$ steps ahead. These models are a GRNN, a GNN and a RNN. Using different amounts of training data, our goal is to compare how well these architectures generalize on the test set. The GRNN architecture takes in single-feature input sequences ($F_X = 1$) and consists of one recurrent layer with $F_Z = 5$ state features and $K_X = K_Z = 5$ filter taps for both the input-to-state and the state-to-state filters. The state features are mapped to the output using a 1-layer GNN with $K_1 = 1$ and $F_1 = F_Y = 1$, adding up to 155 parameters. The GNN architecture takes in individual samples \mathbf{x}_t from the sequence to predict the sample k steps ahead \mathbf{x}_{t+k} , and is made up of 2 graph convolutional layers with $F_X = 1, F_1 = 8, F_2 = F_Y = 1$ and $K_1 = K_2 = 10$, totaling 160 parameters. Finally, the RNN has one layer and both the input and the output have N features ($F_{\text{in}} = F_{\text{out}} = N$), corresponding to the nodes of the graph; the state has $F_Z = 1$ features, and the number of parameters is equal to 160. The fact that all architectures have roughly the same number of parameters is not a coincidence, and was intended to make sure that comparisons are fair.

All architectures were trained 25 times, over 5 different graphs and 5 different dataset realizations. The number of training epochs was 10 and the learning rate 10^{-3} . In the first set of experiments, the size of the training, validation and test sets were 10000, 2400 and 200 sample sequences respectively, and training was done in batches of 100. The mean test rRMSEs and corresponding standard deviations for each architecture are presented in Figure 2b, and the training

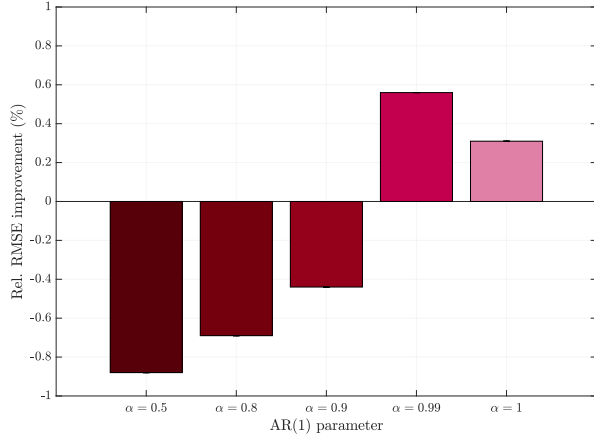


Figure 3. Relative RMSE improvement of t-GGRNN over GRNN on AR diffusion process given by $\mathbf{x}_t = \alpha \mathbf{x}_t + \mathbf{w}_t$ for various values of α .

rRMSE of each architecture versus the number of training steps in Figure 2a. After 10 epochs, the GRNN outperforms the GNN in almost 20 p.p., but the GRNN and RNN achieve roughly the same performance, which makes sense considering that the solution space searched by the GRNN is a subset of that searched by the RNN. On the other hand, Figure 2a shows that the GRNN architecture explores this solution space more efficiently and, consequently, trains faster. This observation is corroborated by the results obtained in the second set of experiments, where the size of the training and validation sets was cut by half. As seen in Figure 2c, when less training data is available the advantages of the additional structure carried by GRNNs are more perceptible, with the GRNN outperforming the RNN in over 10 percentage points even though their number of parameters is exactly the same.

B. k -step prediction: AR(1) process and time gating

In this experiment, \mathcal{G} is an SBM graph with $N = 20$ nodes, $c = 2$ communities, intra-community probability $p_{c_i c_i} = 0.8$ and inter-community probability $p_{c_i c_j} = 0.2$. The graph process is an AR(1) process with parameter $0 < \alpha \leq 1$,

$$\mathbf{x}_t = \alpha \mathbf{x}_{t-1} + \mathbf{w}_t \quad (30)$$

where $\mathbf{w}_t \in \mathbb{R}^N$ is once again a zero-mean Gaussian noise with temporal variance $\xi^2 = 0.01$ and spatial variance $\eta^2 = 0.01$. When α is close to 0, this process is weakly correlated in time; when it is close to 1, $\mathbf{x}_t \approx \mathbf{x}_{t-1}$ and the process is strongly correlated. To assess the advantages of time gating (cf. equation (23)) in processes with different levels of temporal correlation, in this experiment we simulate the k -step prediction problem for $k = 10$ and a range of values of α between 0 and 1. The architectures that we compare are a time-gated GRNN and a conventional GRNN with $F_{\mathbf{x}} = 1$, $F_{\mathbf{z}} = 10$ and $K_{\mathbf{x}} = K_{\mathbf{z}} = 4$. In both GRNNs, the state is mapped to the output using a 1-layer GNN with $F_1 = F_{\mathbf{y}} = 1$ and $K_{\text{out}} = 1$.

We report results for 25 runs of this experiment corresponding to 5 different graphs and 5 different datasets for each

graph. The number of training, validation and test samples in each dataset realization were 10000, 2400 and 200, and number of training epochs, batch size and learning rate were 20, 100 and 5×10^{-4} respectively. The relative RMSE improvement of the time-gated GRNN over the basic GRNN is presented in Figure 3 for multiple values of α . We observe that, for small α , the GRNN achieves lower RMSE than the t-GGRNN on average, but t-GGRNN performance improves relative to the GRNN as α increases. This is because, for large α , there is memory *within the process*, that is, within \mathbf{x}_t . In processes with this kind of “built-in memory”, the state \mathbf{z}_t is less important than the instantaneous input \mathbf{x}_t ; the forget gate $\tilde{\mathcal{G}}_t$ thus helps to tune this importance, partially shutting off \mathbf{z}_t and making it easier to learn long term dependencies in processes of this sort.

C. k -step prediction: graph diffusion and node gating

Consider an SBM graph \mathcal{G} with $N = 20$ nodes, $C = 2$ communities, and inter-community and intra-community probabilities $p_{c_i c_j} = 0.8$ and $p_{c_i c_i} = 0.1$. In this experiment, we simulate a graph diffusion process where the GSO $\mathbf{S} \in \mathbb{R}^{N \times N}$ is exponentiated by $\alpha \in (0, 1]$,

$$\mathbf{x}_t = \mathbf{S}^\alpha \mathbf{x}_{t-1} + \mathbf{w}_t \quad (31)$$

and where $\mathbf{w}_t \in \mathbb{R}^N$ a zero-mean Gaussian with temporal variance $\xi^2 = 0.01$ and spatial variance $\eta^2 = 0.01$. The role of α is to control the process’ “spatial correlation”. The idea is that, the closer α is to 1, the more correlated the process is across nodes connected by edges of the graph.

To assess the advantages of node gating in spatially correlated graph processes, we simulate this process for a range of values of α and train a GRNN and a node-gated GRNN to predict the diffused signals $k = 10$ steps ahead. Both the GRNN and n-GGRNN take in input sequences with $F_{\mathbf{x}} = 1$ input feature and have $F_{\mathbf{z}} = 10$ state features and $K_{\mathbf{x}} = K_{\mathbf{z}} = 4$ filter taps. The state features are mapped to the output using a 1-layer GNN with $F_1 = F_{\mathbf{y}} = 1$ and $K_1 = 1$. The GRNN and the n-GRNN were trained 25 times over 5 different graphs and 5 different datasets for each graph, each dataset consisting of 10000 training, 2400 validation and 200 test samples. The learning rate, number of epochs and batch size were 10^{-3} , 10 and 100. The average relative RMSE improvement of the node gated architecture over the basic GRNN architecture can be seen in Figure 4 for $\alpha = 0.005, 0.01, 0.1, 0.2, 0.5, 1$.

When α is closer to 0, the state \mathbf{z}_t is more informative than \mathbf{x}_t , and we see the effect of the input gate shutting off the input; when α is closer to 1, the input \mathbf{x}_t is more informative, and it is now the forget gate that shuts off the state. In the mid-range, the effects of both gates are combined, yielding the largest performance improvements of the n-GGRNN over the GRNN.

D. k -step prediction: covariance graphs and edge gating

In this experiment, the graph \mathcal{G} is a n -nearest-neighbor covariance graph with $N = 20$ nodes, and the diffusion process is a simple graph diffusion given by

$$\mathbf{x}_t = \mathbf{S} \mathbf{x}_{t-1} + \mathbf{w}_t \quad (32)$$

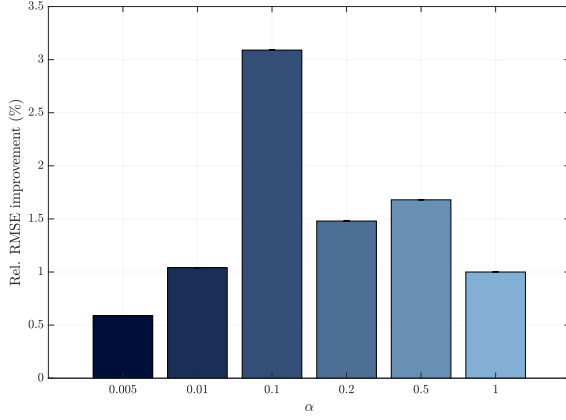


Figure 4. Relative RMSE improvement of n-GGRNN over GRNN on graph diffusion process given by $\mathbf{x}_t = \mathbf{S}^\alpha \mathbf{x}_t + \mathbf{w}_t$ for various values of α .

where $\mathbf{w}_t \in \mathbb{R}^N$ a zero-mean Gaussian with temporal variance $\xi^2 = 0.01$ and spatial variance $\eta^2 = 0.01$. The GSO \mathbf{S} is the sample covariance of the \mathbf{x}_0 in the training set, which consist of 10000 samples taken from a multivariate normal distribution with mean $\boldsymbol{\mu} = \mathbf{1}$ and true covariance matrix $[\Sigma]_{ii} = 3$, $[\Sigma]_{ij} = 1$ for $1 \leq i, j \leq 20$, $i \neq j$. This procedure yields complete graphs and so, to assess the effects of edge gating in graphs with different levels of connectivity, we set each node's maximum number of neighbors to n , and vary n between 5 and 20.

The compared architectures are an edge-gated GRNN and a basic GRNN, both with $F_{\mathbf{X}} = 1$, $F_{\mathbf{Z}} = 10$ and $K_{\mathbf{X}} = K_{\mathbf{Z}} = 4$ and followed by an output GNN consisting of one layer with $K_{\mathbf{Y}} = 1$ and $F_1 = F_{\mathbf{Y}} = 1$. These architectures were trained on 5 different graphs, with 5 different diffusion datasets each. In all realizations, the learning rate was 10^{-3} , and training was done in 10 epochs and batches of 100 samples. The number of samples in the validation and test sets were 2400 and 200 respectively.

The results of this experiment are presented in Figure 5, in terms of the relative RMSE improvement of the edge gated architecture over the GRNN. For smaller number of neighbors n , the e-GGRNN obtains larger relative RMSE than the basic GRNN on average, but as n increases this behavior gradually shifts and the effects of edge gating can be perceived. In particular, for $n = 15$ and $n = 20$ the edge-gated GRNN outperforms the GRNN.

E. Earthquake epicenter estimation

We use seismic wave data from the Geonet database [46] to predict the region of origin of 2289 earthquakes registered between June 17, 2019 and July 17, 2019 in New Zealand. The graph \mathcal{G} is a 3-nearest neighbor network constructed from the coordinates of $N = 59$ seismographs, and the input data consists of 10s and 20s seismic wave readings sampled at 2 Hz and registered immediately before the seisms.

The prediction space \mathcal{Y} corresponds to $C = 11$ class labels, each pertaining to a different region of New Zealand. Using 10 different data splits of 1648 earthquakes for training, 412 for

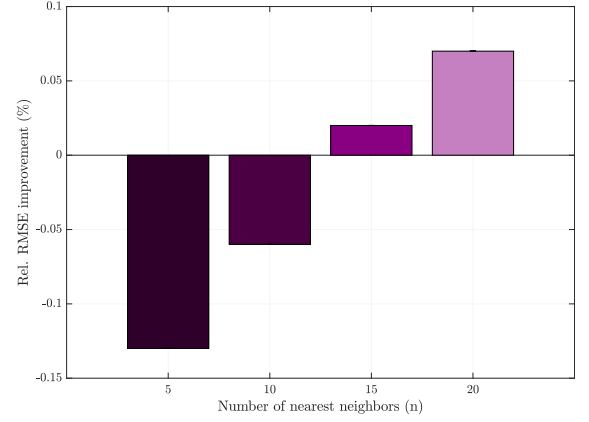


Figure 5. Relative RMSE improvement of e-GGRNN over GRNN on diffusion process on covariance graphs with 5, 10, 15 and 20 nearest neighbors.

Number of parameters in the 10s case	
GNN	1 layer, $F_{\mathbf{X}} = 20$, $F_1 = 21$, $K_1 = 4$
RNN	1 layer, $F_{\mathbf{X}} = 1$, $F_{\mathbf{Z}} = 21$
All GRNNs	$F_{\mathbf{X}} = 1$, $F_{\mathbf{Z}} = 20$, $K_{\mathbf{X}} = 4$, $K_{\mathbf{Z}} = 4$

Table I: Number of parameters of the GNN, RNN and all GRNN architectures for the earthquake epicenter estimation experiment using 10s-long seismic waves.

validation and 229 for test, we simulate 6 different models: a GNN, a RNN, a basic GRNN, and time, node and edge-gated versions of the GRNN. The hyperparameters of these architectures are presented in Tables I and II for the 10s and 20s case, and were set to ensure roughly the same number of parameters in the inner layers of these architectures (except for the time, node, and edge-gated architectures, which have one additional GRNN per gate). Notice that in both the 10s and the 20s scenarios the number of parameters of the RNN and of the GRNNs is unchanged, but the number of parameters of the GNN has to be adjusted because the increase in the length of the input sequence corresponds to an increase in the number of input features for the GNN.

The average test accuracies are reported in Tables III and IV. Every graph recurrent architecture outperforms both the GNN and RNN by a significant margin, regardless of the duration of the waves; in particular, they improve upon the RNN in over 5 percentage points, which corroborates the observation made in subsection VI-A that even if the RNN has more representative power than the GRNN, it searches the representation space less efficiently because it lacks structural information about the graph. This presents a disadvantage in “harder”, real-world problems, where there is a limited amount of training data (because data cannot be synthetically generated). As for gating, although all other gated architectures achieve roughly the same accuracy as the basic GRNN, edge gating improves performance in around 5% on average (~ 2 p.p.). This is telling of the advantages of edge gating even in graphs that are not highly connected, as in the seismograph network each node is only connected to its 3 closest neighbors.

Number of parameters in the 20s case	
GNN	1 layer, $F_{\mathbf{X}} = 40, F_1 = 11, K_1 = 4$
RNN	1 layer, $F_{\mathbf{X}} = 1, F_{\mathbf{Z}} = 21$
All GRNNs	$F_{\mathbf{X}} = 1, F_{\mathbf{Z}} = 20, K_{\mathbf{X}} = 4, K_{\mathbf{Z}} = 4$

Table II: Number of parameters of the GNN, RNN and all GRNN architectures for the earthquake epicenter estimation experiment using 20s-long seismic waves.

Earthquake region prediction accuracy (%) - 10s waves					
GNN	RNN	GRNN	t-GGRNN	n-GGRNN	e-GGRNN
24.84	34.69	40.76	40.61	40.39	42.71

Table III: Average earthquake region prediction accuracy (%) achieved by the GNN, RNN, GRNN, t-GGRNN, n-GGRNN and e-GGRNN for 10s-long seismic waves.

VII. CONCLUSIONS

In this paper, we have introduced a graph recurrent neural network tailored to learning problems involving graph processes. Merging the recurrent architecture of RNNs with graph convolutional layers, GRNNs are able to take both the sequential structure of data and the underlying graph topology into account. We have shown that GRNNs are Lipschitz stable to graph perturbations with a Lipschitz constant that is polynomial on the length of the graph processes considered. The GRNN architecture was also extended to include three gating strategies: (i) time gating, which enables encoding long term time dependencies without assigning them exponentially smaller/larger weights; (ii) node gating, in which each node has a gate and the graph structure is leveraged to control spatial dependencies on the graph; and (iii) edge gating, which achieves the same purpose but by assigning gates to edges instead. The advantages of these architectures were demonstrated in both a synthetic problem of k -step prediction and a real-world problem that used seismic wave readings to predict the region of origin of earthquakes in New Zealand. GRNN architectures outperformed GNNs and RNNs in both settings, attesting to the importance of incorporating the full structure of data in the design of more efficient learning architectures.

APPENDIX A PROOF OF PROPOSITION 1

Proof of Proposition 1. Since the permutation matrix $\mathbf{P} \in \mathcal{P}$ is orthogonal, we have $\mathbf{P}^\top \mathbf{P} = \mathbf{P} \mathbf{P}^\top$, which implies

$$\tilde{\mathbf{S}}^k = (\mathbf{P}^\top \mathbf{S} \mathbf{P})^k = \mathbf{P}^\top \mathbf{S}^k \mathbf{P}. \quad (33)$$

Writing $\mathbf{A}(\tilde{\mathbf{S}})$ as in (4), we get

$$\mathbf{A}(\tilde{\mathbf{S}}) = \mathbf{P}^\top \mathbf{A}(\mathbf{S}) \mathbf{P} \quad (34)$$

and so applying $\mathbf{A}(\tilde{\mathbf{S}})$ to $\tilde{\mathbf{x}} = \mathbf{P}^\top \mathbf{x}$ yields

$$\mathbf{A}(\tilde{\mathbf{S}})\tilde{\mathbf{x}} = \mathbf{P}^\top \mathbf{A}(\mathbf{S}) \mathbf{P} \mathbf{P}^\top \mathbf{x} = \mathbf{P}^\top \mathbf{A}(\mathbf{S}) \mathbf{x}. \quad (35)$$

Graph convolutions are thus permutation equivariant. Using (5), we can then write $\tilde{\mathbf{z}}_t$ as

$$\tilde{\mathbf{z}}_t = \sigma(\mathbf{A}(\tilde{\mathbf{S}})\tilde{\mathbf{x}}_t + \mathbf{B}(\tilde{\mathbf{S}})\tilde{\mathbf{z}}_{t-1}) \quad (36)$$

$$= \sigma(\mathbf{P}^\top \mathbf{A}(\mathbf{S}) \mathbf{x}_t + \mathbf{P}^\top \mathbf{B}(\mathbf{S}) \mathbf{z}_{t-1}) \quad (37)$$

$$= \mathbf{P}^\top \sigma(\mathbf{A}(\mathbf{S}) \mathbf{x}_t + \mathbf{B}(\mathbf{S}) \mathbf{z}_{t-1}) = \mathbf{P}^\top \mathbf{z}_t \quad (38)$$

Earthquake region prediction accuracy (%) - 20s waves					
GNN	RNN	GRNN	t-GGRNN	n-GGRNN	e-GGRNN
25.63	35.07	40.80	40.35	40.04	42.93

Table IV: Average earthquake region prediction accuracy (%) achieved by the GNN, RNN, GRNN, t-GGRNN, n-GGRNN and e-GGRNN for 20s-long seismic waves.

where the second-to-last equality follows from the fact that σ is pointwise and hence permutation equivariant. Since ρ is also pointwise, by a similar reasoning we have $\tilde{\mathbf{y}}_t = \rho(\mathbf{C}(\tilde{\mathbf{S}})\tilde{\mathbf{z}}_t) = \mathbf{P}^\top \rho(\mathbf{C}(\mathbf{S})\mathbf{z}_t) = \mathbf{P}^\top \mathbf{y}_t$. \square

APPENDIX B PROOF OF THEOREM 1

Lemma 1. Let $\mathbf{S} = \mathbf{V} \mathbf{\Lambda} \mathbf{V}^\mathbf{H}$ and $\tilde{\mathbf{S}}$ be graph shift operators. Let $\mathbf{E} = \mathbf{U} \mathbf{M} \mathbf{U}^\mathbf{H} \in \mathcal{E}(\mathbf{S}, \tilde{\mathbf{S}})$ be a relative perturbation matrix (cf. Definition 1) whose norm is such that

$$d(\mathbf{S}, \tilde{\mathbf{S}}) \leq \|\mathbf{E}\| \leq \varepsilon.$$

For an integral Lipschitz filter (cf. Definition 2) with integral Lipschitz constant C , the operator distance modulo permutation between filters $\mathbf{H}(\mathbf{S})$ and $\mathbf{H}(\tilde{\mathbf{S}})$ satisfies

$$\|\mathbf{H}(\mathbf{S}) - \mathbf{H}(\tilde{\mathbf{S}})\|_{\mathcal{P}} \leq 2C \left(1 + \delta \sqrt{N}\right) \varepsilon + \mathcal{O}(\varepsilon^2) \quad (39)$$

with $\delta := (\|\mathbf{U} - \mathbf{V}\|_2 + 1)^2 - 1$ standing for the eigenvector misalignment between shift operator \mathbf{S} and error matrix \mathbf{E} .

Proof. See [21, Theorem 3]. \square

Proof of Theorem 1. Without loss of generality, assume $\mathbf{P} = \mathbf{I}$ in (14) and write $\tilde{\mathbf{S}} = \mathbf{S} + \mathbf{E} \mathbf{S} + \mathbf{S} \mathbf{E}^\top$, $\tilde{\mathbf{A}} = \mathbf{A}(\tilde{\mathbf{S}})$, $\tilde{\mathbf{B}} = \mathbf{B}(\tilde{\mathbf{S}})$ and $\tilde{\mathbf{C}} = \mathbf{C}(\tilde{\mathbf{S}})$. From (6), we can write

$$\|\mathbf{y}_t - \tilde{\mathbf{y}}_t\| = \|\rho(\mathbf{C} \mathbf{z}_t) - \rho(\tilde{\mathbf{C}} \tilde{\mathbf{z}}_t)\| \leq \|\mathbf{C} \mathbf{z}_t - \tilde{\mathbf{C}} \tilde{\mathbf{z}}_t\| \quad (40)$$

since $\rho(\cdot)$ is normalized Lipschitz. Adding and subtracting $\mathbf{C} \tilde{\mathbf{z}}$ on the right-hand side of (40), and using both the triangle and Cauchy-Schwarz inequalities, we get

$$\|\mathbf{y}_t - \tilde{\mathbf{y}}_t\| \leq \|\mathbf{C}\| \|\mathbf{z}_t - \tilde{\mathbf{z}}_t\| + \|\mathbf{C} - \tilde{\mathbf{C}}\| \|\tilde{\mathbf{z}}_t\|. \quad (41)$$

The norm of \mathbf{C} is assumed bounded, and Lemma 1 gives a bound to $\|\mathbf{C} - \tilde{\mathbf{C}}\|$. Using (5), we can write

$$\|\mathbf{z}_t - \tilde{\mathbf{z}}_t\| = \|\sigma(\mathbf{A} \mathbf{x}_t + \mathbf{B} \mathbf{z}_{t-1}) - \sigma(\tilde{\mathbf{A}} \mathbf{x}_t + \tilde{\mathbf{B}} \tilde{\mathbf{z}}_{t-1})\| \quad (42)$$

$$\leq \|\mathbf{A} \mathbf{x}_t + \mathbf{B} \mathbf{z}_{t-1} - (\tilde{\mathbf{A}} \mathbf{x}_t + \tilde{\mathbf{B}} \tilde{\mathbf{z}}_{t-1})\| \quad (43)$$

$$\leq \|\mathbf{A} - \tilde{\mathbf{A}}\| \|\mathbf{x}_t\| + \|\mathbf{B} \mathbf{z}_{t-1} - \tilde{\mathbf{B}} \tilde{\mathbf{z}}_{t-1}\| \quad (44)$$

where the first inequality follows from the fact that $\sigma(\cdot)$ is also normalized Lipschitz and the second from the triangle and Cauchy-Schwarz inequalities respectively. The norm difference $\|\mathbf{A} - \tilde{\mathbf{A}}\|$ is bounded by Lemma 1 and $\|\mathbf{x}_t\| \leq \|\mathbf{x}\|$ for all t , so we move onto deriving a bound for the second summand of (44). We rewrite it as

$$\|\mathbf{B} \mathbf{z}_{t-1} + \tilde{\mathbf{B}} \tilde{\mathbf{z}}_{t-1} - \tilde{\mathbf{B}} \tilde{\mathbf{z}}_{t-1} - \tilde{\mathbf{B}} \tilde{\mathbf{z}}_{t-1}\| \quad (45)$$

$$\leq \|\mathbf{B}\| \|\mathbf{z}_{t-1} - \tilde{\mathbf{z}}_{t-1}\| + \|\mathbf{B} - \tilde{\mathbf{B}}\| \|\tilde{\mathbf{z}}_{t-1}\| \quad (46)$$

which results in a recurrence relationship between $\|\mathbf{z}_t - \tilde{\mathbf{z}}_t\|$ and $\|\mathbf{z}_{t-1} - \tilde{\mathbf{z}}_{t-1}\|$. Expanding this recurrence, we obtain

$$\begin{aligned} \|\mathbf{z}_t - \tilde{\mathbf{z}}_t\| &\leq \sum_{i=0}^{t-1} \|\mathbf{B}\|^i \|\mathbf{A} - \tilde{\mathbf{A}}\| \|\mathbf{x}\| \\ &\quad + \|\mathbf{B}\|^t \|\mathbf{z}_0 - \tilde{\mathbf{z}}_0\| + \|\mathbf{B} - \tilde{\mathbf{B}}\| \sum_{i=1}^t \|\tilde{\mathbf{z}}_{t-i}\| \\ &\leq \sum_{i=0}^{t-1} \|\mathbf{B}\|^i \|\mathbf{A} - \tilde{\mathbf{A}}\| \|\mathbf{x}\| + \|\mathbf{B} - \tilde{\mathbf{B}}\| \sum_{i=0}^{t-1} \|\tilde{\mathbf{z}}_i\| \end{aligned}$$

where the second inequality follows from $\mathbf{z}_0 = \tilde{\mathbf{z}}_0$. Now it suffices to bound $\|\mathbf{z}_i\|$ for any given $i > 0$. Writing \mathbf{z}_t as in (5) and observing that, because $\sigma(\cdot)$ is normalized Lipschitz and $\sigma(0) = 0$, $|\sigma(x)| < |x|$, we can use the triangle and Cauchy-Schwarz inequalities to write

$$\begin{aligned} \|\mathbf{z}_i\| &\leq \|\mathbf{A}\| \|\mathbf{x}_i\| + \|\mathbf{B}\| \|\mathbf{z}_{i-1}\| \leq \dots \\ &\leq \sum_{j=0}^{i-1} \|\mathbf{B}\|^j \|\mathbf{A}\| \|\mathbf{x}\| + \|\mathbf{B}\|^i \|\mathbf{z}_0\| \end{aligned}$$

for $i > 0$. Substituting this in (46), we get

$$\|\mathbf{z}_t - \tilde{\mathbf{z}}_t\| \leq \|\mathbf{A} - \tilde{\mathbf{A}}\| \|\mathbf{x}\| \sum_{i=0}^{t-1} \|\mathbf{B}\|^i \quad (47)$$

$$+ \|\mathbf{B} - \tilde{\mathbf{B}}\| \left(\|\tilde{\mathbf{A}}\| \|\mathbf{x}\| \sum_{i=1}^{t-1} \sum_{j=0}^{i-1} \|\tilde{\mathbf{B}}\|^j + \|\mathbf{z}_0\| \sum_{i=0}^{t-1} \|\tilde{\mathbf{B}}\|^i \right). \quad (48)$$

Finally, substituting equations (46) and (47) in (41) gives

$$\begin{aligned} \|\mathbf{y}_t - \tilde{\mathbf{y}}_t\| &\leq \|\mathbf{C}\| \left[\|\mathbf{A} - \tilde{\mathbf{A}}\| \|\mathbf{x}\| \sum_{i=0}^{t-1} \|\mathbf{B}\|^i \right. \\ &\quad + \|\mathbf{B} - \tilde{\mathbf{B}}\| \left(\|\tilde{\mathbf{A}}\| \|\mathbf{x}\| \sum_{i=1}^{t-1} \sum_{j=0}^{i-1} \|\tilde{\mathbf{B}}\|^j + \|\mathbf{z}_0\| \sum_{i=0}^{t-1} \|\tilde{\mathbf{B}}\|^i \right) \\ &\quad \left. + \|\mathbf{C} - \tilde{\mathbf{C}}\| \left[\sum_{i=0}^{t-1} \|\tilde{\mathbf{B}}\|^i \|\tilde{\mathbf{A}}\| \|\mathbf{x}\| + \|\tilde{\mathbf{B}}\|^t \|\mathbf{z}_0\| \right] \right]. \end{aligned}$$

This expression can be simplified by applying Lemma 1 to the norm differences $\|\mathbf{A} - \tilde{\mathbf{A}}\|$, $\|\mathbf{B} - \tilde{\mathbf{B}}\|$ and $\|\mathbf{C} - \tilde{\mathbf{C}}\|$, and by recalling that $\|\mathbf{A}\| = \|\mathbf{B}\| = \|\mathbf{C}\| = 1$, $\|\mathbf{x}\| = 1$ and $\mathbf{z}_0 = \mathbf{0}$. Denoting by $C = \max\{C_A, C_B, C_C\}$ the maximum filter Lipschitz constant, we recover (19) with $\mathbf{P} = \mathbf{I}$,

$$\|\mathbf{y}_t - \tilde{\mathbf{y}}_t\| \leq C(1 + \sqrt{N}\delta)(t^2 + 3t)\varepsilon + \mathcal{O}(\varepsilon^2) \quad (49)$$

which completes the proof. \square

REFERENCES

- [1] L. Ruiz, F. Gama, and A. Ribeiro, "Gated graph convolutional recurrent neural networks," in *27th Eur. Signal Process. Conf.* Spain: IEEE, 2-6 Sep. 2019.
- [2] Y. Miao, M. Gowayyed, and F. Metze, "EESSEN: End-to-end speech recognition using deep RNN models and WFST-based decoding," in *IEEE Workshop on Automatic Speech Recognition and Understanding*, Scottsdale, AZ: IEEE, 13-17 Dec. 2015, pp. 167-174.
- [3] A. Graves, A. Mohamed, and G. Hinton, "Speech recognition with deep recurrent neural networks," in *2013 IEEE Int. Conf. Acoust., Speech and Signal Process.* Vancouver, BC: IEEE, 26-31 May 2013, pp. 6645-6649.
- [4] A. Krizhevsky, I. Sutskever, and G. E. Hinton, "Imagenet classification with deep convolutional neural networks," in *25th Conf. Neural Inform. Process. Syst.*, Spain, 12-17 Dec. 2011, pp. 1097-1105.
- [5] S. S. Baboo and I. K. Shereef, "An efficient weather forecasting system using artificial neural network," *International Journal of Environmental Science and Development*, vol. 1, no. 4, p. 321, 2010.
- [6] U. R. Acharya, H. Fujita, S. L. Oh, Y. Hagiwara, J. H. Tan, and M. Adam, "Application of deep convolutional neural network for automated detection of myocardial infarction using ecg signals," *Information Sciences*, vol. 415, pp. 190-198, 2017.
- [7] Y. LeCun, Y. Bengio, and G. Hinton, "Deep learning," *Nature*, vol. 521, no. 7553, pp. 85-117, 2015.
- [8] C.-C. J. Kuo, "The CNN as a guided multilayer RECOs transform," *IEEE Signal Process. Mag.*, vol. 34, no. 3, pp. 81-89, May 2017.
- [9] J. Yosinski, J. Clune, Y. Bengio, and H. Lipson, "How transferable are features in deep neural networks?" in *Conf. Neural Inform. Process. Syst.*, Montreal, QC, 8-13 Dec. 2014, pp. 3320-3328.
- [10] T. N. Kipf and M. Welling, "Semi-supervised classification with graph convolutional networks," in *5th Int. Conf. Learning Representations*. Toulon, France: Assoc. Comput. Linguistics, 24-26 Apr. 2017, pp. 1-14.
- [11] M. Defferrard, X. Bresson, and P. Vandergheynst, "Convolutional neural networks on graphs with fast localized spectral filtering," in *30th Conf. Neural Inform. Process. Syst.* Barcelona, Spain: Neural Inform. Process. Foundation, 5-10 Dec. 2016, pp. 3844-3858.
- [12] F. Gama, A. G. Marques, G. Leus, and A. Ribeiro, "Convolutional neural network architectures for signals supported on graphs," *IEEE Trans. Signal Process.*, vol. 67, no. 4, pp. 1034-1049, Feb. 2019.
- [13] R. Pascanu, C. Gulcehre, K. Cho, and Y. Bengio, "How to construct deep recurrent neural networks," *arXiv:1312.6026 [cs.NE]*, 24 Apr. 2014. [Online]. Available: <http://arxiv.org/abs/1312.6026>
- [14] A. Graves, "Generating sequences with recurrent neural networks," *arXiv:1308.0850 [cs.NE]*, 5 June 2014. [Online]. Available: <http://arxiv.org/abs/1308.0850>
- [15] M. Schuster and K. K. Paliwal, "Bidirectional recurrent neural networks," *IEEE Trans. Signal Process.*, vol. 45, no. 11, pp. 2673-2681, 1997.
- [16] I. Goodfellow, Y. Bengio, and A. Courville, *Deep Learning*, ser. The Adaptive Computation and Machine Learning Series. Cambridge, MA: The MIT Press, 2016.
- [17] N. Perraudin and P. Vandergheynst, "Stationary signal processing on graphs," *IEEE Trans. Signal Process.*, vol. 65, no. 13, pp. 3462-3477, July 2017.
- [18] F. Grassi, A. Loukas, N. Perraudin, and B. Ricaud, "A time-vertex signal processing framework: Scalable processing and meaningful representations for time-series on graphs," *IEEE Trans. Signal Process.*, vol. 66, no. 3, pp. 817-829, Feb. 2018.
- [19] F. Gama, A. G. Marques, G. Leus, and A. Ribeiro, "Convolutional graph neural networks," in *53rd Asilomar Conf. Signals, Systems and Comput.* Pacific Grove, CA: IEEE, 3-6 Nov. 2019.
- [20] L. Ruiz, F. Gama, A. G. Marques, and A. Ribeiro, "Invariance-preserving localized activation functions for graph neural networks," *IEEE Trans. Signal Process.*, vol. 68, no. 1, pp. 127-141, Jan. 2020.
- [21] F. Gama, J. Bruna, and A. Ribeiro, "Stability properties of graph neural networks," *arXiv:1905.04497v2 [cs.LG]*, 4 Sep. 2019. [Online]. Available: <http://arxiv.org/abs/1905.04497>
- [22] Y. Li, R. Yu, C. Shahabi, and Y. Liu, "Diffusion convolutional recurrent neural network: Data-driven traffic forecasting," in *Int. Conf. Learning Representations 2018*. Vancouver, BC: Assoc. Comput. Linguistics, 30 Apr.-3 May 2018.
- [23] J. Zhang, X. Shi, J. Xie, H. Ma, I. King, and D.-Y. Yeung, "GaAN: Gated attention networks for learning on large and spatiotemporal graphs," in *Conf. Uncertainty Artificial Intell. 2018*, no. 139. Monterey, CA: Assoc. Uncertainty Artificial Intell., 6-10 Aug. 2018.
- [24] B. Yu, H. Yin, and Z. Zhu, "Spatio-temporal graph convolutional networks: A deep learning framework for traffic forecasting," in *27th Int. Joint Conf. Artificial Intell.* Stockholm, Sweden: Eur. Assoc. Artificial Intell., 13-19 July 2018, pp. 3634-3640.
- [25] Y. Seo, M. Defferrard, P. Vandergheynst, and X. Bresson, "Structured sequence modeling with graph convolutional recurrent networks," in *32nd Conf. Neural Inform. Process. Syst.* Montreal, QC: Springer, 3-8 Dec. 2018, pp. 362-373.
- [26] Y. Li, D. Tarlow, M. Brockschmidt, and R. Zemel, "Gated graph sequence neural networks," *arXiv:1511.05493 [cs.LG]*, 22 Sep. 2017. [Online]. Available: <http://arxiv.org/abs/1511.05493>
- [27] V. N. Ioannidis, A. G. Marques, and G. B. Giannakis, "A recurrent graph neural network for multi-relational data," in *44th IEEE Int. Conf.*

- Acoust., Speech and Signal Process.* Brighton, UK: IEEE, 12-17 May 2019.
- [28] C. Baziotis, N. Pelekis, and C. Doulkeridis, “DataStories at SemEval-2017 Task 4: Deep LSTM with attention for message-level and topic-based sentiment analysis,” in *Proceedings of the 11th International Workshop on Semantic Evaluation*, Vancouver, BC, Aug. 2017, pp. 747–754.
 - [29] A. Sandryhaila and J. M. F. Moura, “Discrete signal processing on graphs,” *IEEE Trans. Signal Process.*, vol. 61, no. 7, pp. 1644–1656, Apr. 2013.
 - [30] D. I. Shuman, S. K. Narang, P. Frossard, A. Ortega, and P. Vandergheynst, “The emerging field of signal processing on graphs: Extending high-dimensional data analysis to networks and other irregular domains,” *IEEE Signal Process. Mag.*, vol. 30, no. 3, pp. 83–98, May 2013.
 - [31] A. Heimowitz and Y. C. Eldar, “A unified view of diffusion maps and signal processing on graphs,” in *2017 Int. Conf. Sampling Theory and Appl.* Tallin, Estonia: IEEE, 3-7 July 2017, pp. 308–312.
 - [32] J. Du, J. Shi, S. Kar, and J. M. F. Moura, “On graph convolution for graph CNNs,” in *2018 IEEE Data Sci. Workshop.* Lausanne, Switzerland: IEEE, 4-6 June 2018, pp. 239–243.
 - [33] S. Segarra, A. G. Marques, and A. Ribeiro, “Optimal graph-filter design and applications to distributed linear network operators,” *IEEE Trans. Signal Process.*, vol. 65, no. 15, pp. 4117–4131, Aug. 2017.
 - [34] F. Gama and A. Ribeiro, “Ergodicity in stationary graph processes: A weak law of large numbers,” *IEEE Trans. Signal Process.*, vol. 67, no. 10, pp. 2761–2774, May 2019.
 - [35] F. Gama, E. Isufi, A. Ribeiro, and G. Leus, “Controllability of bandlimited graph processes over random time-varying graphs,” *arXiv:1904.10089v1 [cs.SY]*, 22 Apr. 2019. [Online]. Available: <http://arxiv.org/abs/1904.10089>
 - [36] E. Isufi, F. Gama, and A. Ribeiro, “Generalizing graph convolutional neural networks with edge-variant recursions on graphs,” in *27th Eur. Signal Process. Conf.* A Coruña, Spain: Eur. Assoc. Signal Process., 2-6 Sep. 2019.
 - [37] F. Gama, J. Bruna, and A. Ribeiro, “Stability of graph scattering transforms,” in *33rd Conf. Neural Inform. Process. Syst.* Vancouver, BC: Neural Inform. Process. Syst. Foundation, 8-14 Dec. 2019.
 - [38] A. Sandryhaila and J. M. F. Moura, “Discrete signal processing on graphs: Frequency analysis,” *IEEE Trans. Signal Process.*, vol. 62, no. 12, pp. 3042–3054, June 2014.
 - [39] I. Daubechies, *Ten Lectures on Wavelets*, ser. CBMS-NSF Regional Conf. Series Appl. Math. Philadelphia, PA: SIAM, 1992, vol. 61.
 - [40] R. Pascanu, T. Mikolov, and Y. Bengio, “On the difficulty of training recurrent neural networks,” in *Int. Conf. Mach. Learning*, Atlanta, GA, 16-21 June 2013, pp. 1310–1318.
 - [41] Y. Bengio, P. Simard, and P. Frasconi, “Learning long-term dependencies with gradient descent is difficult,” *IEEE Transactions on Neural Networks*, vol. 5, no. 2, pp. 157–166, 1994.
 - [42] F. Gama, G. Leus, A. G. Marques, and A. Ribeiro, “Convolutional neural networks via node-varying graph filters,” in *2018 IEEE Data Sci. Workshop.* Lausanne, Switzerland: IEEE, 4-6 June 2018, pp. 220–224.
 - [43] P. Veličković, G. Cucurull, A. Casanova, A. Romero, P. Liò, and Y. Bengio, “Graph attention networks,” in *Int. Conf. Learning Representations 2018.* Vancouver, BC: Assoc. Comput. Linguistics, 30 Apr.-3 May 2018, pp. 1–12.
 - [44] M. Coutino, E. Isufi, and G. Leus, “Advances in distributed graph filtering,” *IEEE Trans. Signal Process.*, vol. 67, no. 9, pp. 2320–2333, May 2019.
 - [45] E. Isufi, F. Gama, and A. Ribeiro, “Edgenets: edge varying graph neural networks,” *arXiv:2001.07620v1 [cs.LG]*, 21 Jan. 2020. [Online]. Available: <http://arxiv.org/abs/2001.07620>
 - [46] Earthquake Commission, GNS Science, and Land Information New Zealand, “GeoNet,” <https://www.geonet.org.nz/>, 20 Feb. 2019.
 - [47] D. P. Kingma and J. L. Ba, “ADAM: A method for stochastic optimization,” in *3rd Int. Conf. Learning Representations.* San Diego, CA: Assoc. Comput. Linguistics, 7-9 May 2015.